
MaSC: A Masked Similarity Metric for Evaluating Concept-Driven Generation

Patryk Bartkowiak
Adam Mickiewicz University

Lennart Petersen
Kiel University

Bartosz Kotrys
ArtCollect

Dominik Michels
KAUST

Soren Pirk
Kiel University

Wojtek Palubicki
Adam Mickiewicz University

Abstract

Evaluating single-concept personalization in text-to-image diffusion has seen two categories of quantitative metrics: Concept Preservation (CP) measures identity fidelity to a reference while Prompt Following (PF) measures whether the generated scene matches the prompt. Personalization papers have commonly computed these signals using three separate backbones: CLIP-I and DINO for CP, CLIP-T for PF. In this paper, we show that existing metrics fall short of correlating with human perception because they attend to the image as a whole, instead of distinguishing the concept subject from the background. This distinction is important from a human perception point of view as the concept subject in the output image should be very similar to the input concept (CP), whereas the output background should adhere closely to the text prompt (PF). To improve personalization evaluation in this way, we introduce *MaSC*, a unified metric that attends to CP and PF by differentiating concept subject regions. Specifically, given an externally provided foreground concept mask, MaSC computes the CP and PF scores from a single forward pass of a frozen SigLIP2 encoder per image. On DreamBench++ human ratings, MaSC reaches Krippendorff $\alpha = +0.471$ on CP — beating every non-LLM baseline tested (DINOv3, DreamSim, AM-RADIO, DIFT-SDXL, DINO-I, CLIP-I) and GPT-4V, while sitting within $\Delta\alpha = 0.028$ of GPT-4o. To distinguish human perception bias we also evaluate our method, as well as common SOTA baselines, on ORIDa, a real-photo benchmark of identity preservation across physical environments. In this experiment MaSC reaches AUC = 0.992 almost perfectly identifying concept subjects. The PF score, obtained by MaSC without a second encoder forward pass, beats the CLIP-T baseline shipped with DreamBench++. In summary, our comprehensive evaluations demonstrate that MaSC establishes a new state-of-the-art for non-LLM concept preservation, while providing an efficient, unified standard for personalization evaluation. We release MaSC as a pip-installable Python package, alongside independent reproductions of every comparator’s published numbers.

1 Introduction

The ability to personalize text-to-image (T2I) generation to user-supplied subjects has fundamentally transformed generative AI. Methods such as DreamBooth [25], Textual Inversion [6], and IP-Adapter [33] have made subject-driven generation a core research pillar and a standard T2I capability. However, reliably evaluating the success of these personalizations remains a difficult task. A complete evaluation requires capturing two distinct signals: *Concept Preservation* (CP), measuring the identity fidelity of the rendered subject to its reference, and *Prompt Following* (PF), measuring how well the generated scene satisfies the prompt. In the past, the field computed these

signals using three independent backbones inherited from DreamBooth: CLIP-I [20] and DINO [2] for CP, and CLIP-T for PF. Recently, DreamBench++ [19] exposed the severe limitations of this standard trio, revealing that its correlation with human judgments plateaus at a Krippendorff [8] $\alpha \approx 0.3$ on both signals—roughly half the inter-annotator ceiling ($\alpha = 0.658$ for CP, 0.563 for PF). To improve alignment with human judgments, the community has generally taken two approaches: updating the representation encoders, or using Large-Language Models (LLMs) like GPT-4V [18] and GPT-4o [17] as evaluators. The first approach offers only minor improvements, while the second performs well but relies on API-bound, non-differentiable scoring that lacks per-region attribution.

The plateau is not a limitation of the encoders. Global pooling introduces a distinct failure for each evaluation signal: (i) Global cosine for CP averages over the whole image, including background variation that humans correctly ignore when judging identity; (ii) Global text-image cosine for PF combines two distinct quantities: scene adherence to the prompt and the presence of the subject class (a static factor, since the subject is fixed across all test prompts for a given concept). Both failures are consequences of the aggregator and the input space, not the backbone — any encoder under mean or [CLS] pooling inherits them.

These limitations are addressable at inference time, without retraining, via spatial decomposition. We introduce *MaSC*, which uses three lightweight interventions: (i) for each foreground reference patch, taking the maximum cosine against any output patch and averaging under the foreground mask; (ii) applying SigLIP2’s trained attention pooler over the patch tokens with foreground patches masked, yielding a background-only embedding via the pooler’s native masking support; and (iii) excluding the canonical subject name from the prompt, eliminating the static baseline on the text side. A single SigLIP2 SO400M-NaFlex [30] forward pass per image then produces both scores: CP from the patch grid via masked max-cosine, and PF from the masked attention pool against the stripped-prompt text embedding.

MaSC’s spatial decomposition closes most of the performance gap with LLM judges in personalization evaluation. On DreamBench++, *MaSC* is the only non-LLM metric to outperform GPT-4V on CP. On ORIDa [7], a real-photo identity-discrimination benchmark across 50 subjects in 10 environments, *MaSC* is the first non-LLM metric to surpass GPT-4o. Furthermore, the PF score outperforms the CLIP-T baseline shipped with DreamBench++.

Contributions. We propose *MaSC*, a unified personalization metric that produces CP and PF scores from a single SigLIP2 SO400M-NaFlex forward pass per image, given an externally supplied foreground concept mask. We make five contributions: (1) On DreamBench++ human ratings, *MaSC* achieves Krippendorff $\alpha = +0.471$ on CP — outperforming every non-LLM baseline tested, surpassing GPT-4V, and reaching 72% of the human inter-rater ceiling; (2) On ORIDa, *MaSC* is the first non-LLM CP metric to outscore GPT-4o, reaching AUC = 0.992; (3) Same-backbone ablations isolate the contribution to our spatial decomposition strategy rather than the encoder choice, with this approach accounting for $\Delta\alpha = +0.102$ on DreamBench++ and Δ AUC = +0.038 on ORIDa; (4) At a matched parameter budget, *MaSC* outperforms state-of-the-art distilled vision transformers (e.g., AM-RADIO [21]), demonstrating that late-stage explicit masking combined with patch features consistently outperforms internalized mask supervision for personalization evaluation; (5) The PF score, obtained from the same forward pass without an additional vision-encoder call, beats the CLIP-T baseline shipped with DreamBench++.

2 Related Work

Subject-driven text-to-image personalization spans optimization-based methods that fine-tune or augment the generator with a reference subject (DreamBooth, Textual Inversion) and adapter-based methods that inject reference features at inference (IP-Adapter, BLIP-Diffusion [10], Emu2 [28]). While these generative techniques form the core of the personalization literature, our work focuses strictly on the evaluation metrics used to benchmark them. DreamBooth introduced the evaluation protocol of using CLIP-I and DINO-I for image-image fidelity alongside CLIP-T for image-text adherence. This protocol has since been universally adopted. However, DreamBench++ [19] recently benchmarked these metrics against human judgments across an evaluation grid of 7 personalization methods, 150 subjects, and 9 prompts. They demonstrated that with CLIP-I at Krippendorff $\alpha = +0.135$, DINO-I and CLIP-T plateau near $\alpha \approx 0.3$, roughly half the human inter-annotator ceiling ($\alpha = 0.658$ for CP, 0.563 for PF). Our work directly addresses this critical evaluation gap. To

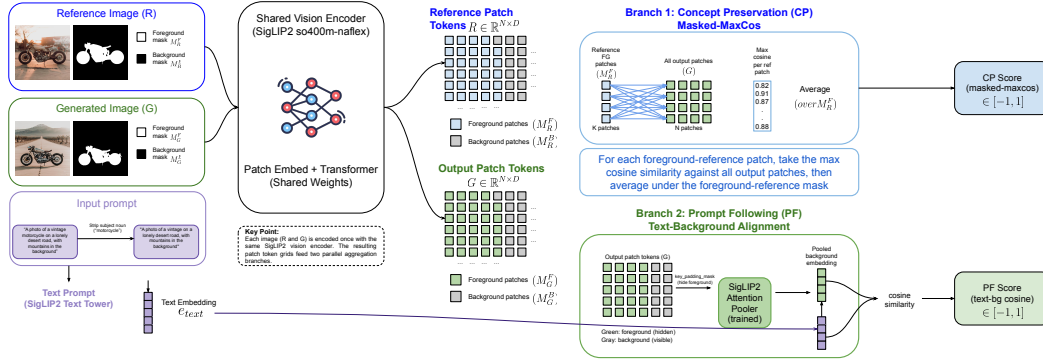


Figure 1: **MaSC pipeline overview**. Reference and generated images are encoded once each by a frozen SigLIP2 SO400M-NaFlex vision tower, producing patch-token grids $R, G \in \mathbb{R}^{N \times D}$. MaSC consumes provided foreground concept masks, denoted $M_R^F, M_G^F \in \{0, 1\}^{H \times W}$. Two branches share the single forward pass. *Branch 1 — Concept Preservation (masked-maxcos)*: for each patch covered by the reference foreground mask (M_R^F), take its maximum cosine similarity against all output patches in G , then average over the foreground-reference patches. *Branch 2 — Prompt Following (Text-Background Alignment)*: the trained SigLIP2 attention pooler is run with foreground patches of G masked from the attention computation, producing a background-only embedding. This is compared via cosine similarity to the text embedding e_{text} of the prompt with the subject noun stripped.

complement DreamBench++, we also evaluate on ORiDA, a real-photo benchmark of identity preservation across natural environments. While ORiDA lacks human ratings, its inclusion of ground-truth per-object segmentation masks makes it an ideal real-world out-of-distribution test for CP. Several non-LLM alternatives have been proposed for image-image fidelity beyond CLIP-I and DINO-I. DreamSim [5] integrates CLIP, DINO, and OpenCLIP backbones and fine-tunes on the NIGHTS triplet dataset for perceptual similarity. DINOv3 [26] is a modern self-supervised vision transformer that updates the original DINO-I baseline. AM-RADIO C-RADIOv4-SO400M is a ViT trained via distillation from SigLIP2-g, DINOv3-7B, and SAM3 [1] simultaneously, internalizing within the encoder weights what MaSC supplies externally as a mask. DIFT [29] extracts dense correspondence features from frozen Stable Diffusion [24] U-Nets. While these methods seek to improve representation through training or architecture, MaSC explores a complementary direction: decomposing the image into concept-specific regions at inference time to isolate identity-relevant features. To address the performance limit of non-LLM metrics, multimodal LLMs have been increasingly employed as judges. DreamBench++ evaluates GPT-4V [18] and GPT-4o [17] on its human-rated subset; GPT-4o achieves CP $\alpha = +0.499$, approaching the human inter-annotator ceiling. Despite their high correlation with humans, these judges are API-bound, non-differentiable, and lack per-region attribution: their scores are scalar outputs that provide no spatial grounding for the judgment. We benchmark against GPT-4V and GPT-4o as the canonical LLM-judge references in the personalization literature. On the PF side, dedicated reward models provide an alternative to LLM judges. ImageReward [32] utilizes a BLIP [11] backbone fine-tuned on pairwise human preferences; HPSv3 [15] extends this paradigm with a Qwen2-VL [31] architecture. VQAScore [12] queries a CLIP-FlanT5 model with ‘Does this figure show prompt?’ and uses the probability of a ‘Yes’ answer as the fidelity score. These are dedicated PF reward models trained on human-preference data. VQAScore ($\sim 3B$) and HPSv3 ($\sim 8B$) wrap larger backbones, while ImageReward ($\sim 360M$) is more compact. Two of the three outperform MaSC on DreamBench++ PF (VQAScore $\alpha = +0.504$, ImageReward $\alpha = +0.441$), while HPSv3 ($\alpha = +0.299$) underperforms MaSC ($\alpha = +0.354$) despite its larger parameter budget. We position the MaSC PF score as a secondary signal obtained from the primary CP forward pass. It outperforms the standard CLIP-T baseline without requiring additional vision-encoder inference or dedicated reward-model training.

3 Method

We now describe MaSC, a unified evaluation metric that uses explicit concept masks to decompose each generated image into subject and background regions, enabling concept preservation and prompt following to be scored from shared frozen SigLIP2 features (Figure 1).

3.1 Setup and Notation

We are given a reference image \mathcal{I}_R , an output image \mathcal{I}_G generated by a personalization method, the natural-language prompt p used to condition the generation, and the subject’s canonical name w (e.g. “kitten”, “piggy bank”). MaSC utilizes explicitly provided concept masks $M_R, M_G \in \{0, 1\}^{H \times W}$ for the two images.

A frozen SigLIP2 SO400M-NaFlex vision tower encodes each image once. The vision tower outputs N patch tokens in \mathbb{R}^D at the NaFlex max-patch budget ($N = 1024$ for our square inputs); we write these as matrices $R, G \in \mathbb{R}^{N \times D}$ and let \tilde{r}_i, \tilde{g}_j denote the ℓ_2 -normalized tokens. The text tower T_θ produces a single embedding in the joint image-text space. The trained image embedding head $\text{Pool}_\theta(\cdot)$ is a single learned-query attention pool over the patch tokens; critically, the pooler accepts a binary suppression mask that excludes arbitrary positions from the attention computation, without changing the trained parameters.

Each $H \times W$ image-resolution mask is downsampled to the patch grid via bilinear interpolation and thresholded at 0.5 to obtain patch-level binary masks $m_R, m_G \in \{0, 1\}^N$. The two scoring branches below share the vision-tower output of each image.

Mask source and filtering. The metric itself is mask-source-agnostic. For our DreamBench++ experiments, we extract M_R and M_G with SAM3 prompted by the canonical concept name w , applied identically to reference and output images. For ORIDa, we use the per-object segmentation masks provided with the dataset. We discard pairs whose foreground masks are too small to carry reliable signal — on DreamBench++, where masks are extracted by SAM3, a near-empty foreground mask typically reflects either a segmentation failure on the reference or a generated output that did not render the subject. This filtering removes degenerate cases where the subject is effectively absent or localization fails, and is applied uniformly across all evaluated methods, independent of the scoring metric. We use a 5% of the image area threshold on DreamBench++: when an output mask falls below 5%, that pair is dropped; when a reference mask falls below 5%, all 9 prompt variants for that subject are dropped, since the reference is reused across them and the failure is intrinsic to the reference rather than to a single output. On ORIDa, the threshold is 0.5%, lower because the provided masks are reliable and the dataset’s real-world objects span a wider scale range than DreamBench++’s synthetic subjects. The PF leaderboard additionally excludes the 20 DreamBench++ “style” subjects, whose prompts describe a visual style rather than a scene; subject-stripping on these prompts produces grammatically malformed fragments. Any segmentation method producing $\{0, 1\}^{H \times W}$ outputs can be substituted for SAM3 without retraining.

3.2 Concept Preservation: masked_maxcos

Let $\mathcal{F}_R = \{i : m_R^{(i)} = 1\}$ index the foreground-reference patches. For each $i \in \mathcal{F}_R$, we take the maximum cosine similarity against any output patch:

$$s_i = \max_{j \in \{1, \dots, N\}} \langle \tilde{r}_i, \tilde{g}_j \rangle.$$

The CP score is the mean of those per-patch best matches under the foreground-reference mask:

$$\text{CP}(R, G, m_R) = \frac{1}{|\mathcal{F}_R|} \sum_{i \in \mathcal{F}_R} s_i. \tag{1}$$

Three design choices are encoded in Equation (1). First, the mask is applied only on the reference side; the output is searched in full, ensuring the metric does not penalize spatial relocation of the concept. Second, the max-cosine inherently measures whether each local patch of the reference concept is present anywhere in the output. This approach degrades gracefully under partial identity preservation, unlike mutual-nearest-neighbor matching, whose strict one-to-one constraint severely

over-penalizes the partial-preservation regime typical of personalization outputs. Third, averaging over the foreground mask aggregates the patch-level matches without overweighting smaller concept regions. As demonstrated in Section 4.4, substituting Equation (1) with mutual-nearest-neighbor matching (using match-count normalization on identical features) drops the Krippendorff α by 0.462 — an aggregation failure that outweighs the contribution of the encoder backbone itself.

3.3 Prompt Following: Background-pool and subject stripping

The PF score is derived via two targeted interventions, one per modality.

Image side: background-only attention pooling. We apply the trained attention pooler to the generated image G while masking its foreground patches from the attention computation, restricting the pool to background tokens only:

$$e_G^{\text{bg}} = \text{Pool}_\theta(G; m_G).$$

Here, m_G serves as a binary suppression mask — positions where $m_G^{(i)} = 1$ are explicitly excluded from the pool. The pooler operates with frozen parameters, only the visibility of the input tokens is altered. Consequently, the output remains in the joint image-text space, enabling direct cosine comparison with text embeddings.

Text side: subject-name stripping. Given the canonical subject name w , we strip w (and any leading articles) from the prompt p using case-insensitive regular expression matching. This string-matching robustly handles multi-word and hyphenated names. Excess whitespace is subsequently collapsed, yielding the stripped prompt $p' = \text{strip}(p, w)$.

Score.

$$\text{PF}(G, m_G, p, w) = \langle \tilde{e}_G^{\text{bg}}, \tilde{T}_\theta(p') \rangle. \quad (2)$$

The intuition: In personalization evaluation, the subject is fixed across all prompts for a given concept. Consequently, whole-image text-image cosine similarity fails to separate the desired signal (scene-prompt alignment) from a persistent baseline. Hiding the foreground from the image pooler suppresses this baseline on the visual side, while stripping the subject name removes the corresponding expectation from the text side. As demonstrated in Section 4.3, a foreground-pooled control yields a negative Krippendorff α , confirming that information strictly contained within the foreground actively degrades prompt-following evaluation.

3.4 Compute Profile

To evaluate a given $(\mathcal{I}_R, \mathcal{I}_G, p, w)$ tuple, MaSC requires: two vision-tower forward passes (one per image, utilizing the $\sim 428\text{M}$ parameter SigLIP2 SO400M-NaFlex encoder), a single execution of the trained attention pooler on the cached output patches with foreground positions suppressed via m_G , and one text-tower forward pass on the stripped prompt. Because the CP branch directly reuses the cached vision features, computing both the CP and PF metrics jointly incurs no additional vision-encoder cost beyond the initial feature extraction.

4 Results

We evaluate MaSC on human-rated personalization benchmarks and real-photo identity-discrimination tasks, comparing it against standard CLIP/DINO metrics, modern non-LLM similarity models, reward-based prompt-following scores, and multimodal LLM judges.

4.1 CP on DreamBench++

Table 1 reports CP α and ρ for MaSC and ten comparators on the 7,135-key DreamBench++ subset — the strictly matched intersection of all standard baselines, both LLM judges, and the new comparator runs. MaSC is the only non-LLM metric to outperform GPT-4V on the benchmark. It trails GPT-4o (the only superior entry) by just $\Delta\alpha = 0.028$, reaching 72% of the human inter-annotator ceiling.

Table 1: Concept Preservation on DreamBench++. Krippendorff α (Kd_o) and Spearman ρ against pooled human ratings on the 7,135-key apples-to-apples subset. **Bold**: ours — the only non-LLM, non-human metric to beat GPT-4V; sits $\Delta\alpha = -0.028$ behind GPT-4o and reaches 72% of the honest human inter-rater ceiling.

#	Metric	Kind	α	ρ
—	<i>Human inter-rater</i>	<i>ceiling</i>	+0.658	+0.653
1	GPT-4o	LLM judge	+0.499	+0.641
2	MaSC	non-LLM	+0.471	+0.611
3	GPT-4V	LLM judge	+0.432	+0.521
4	DreamSim	non-LLM	+0.421	+0.599
5	SigLIP2 SO400M-NaFlex global pool	non-LLM	+0.369	+0.557
6	DINOv3	non-LLM	+0.345	+0.479
7	DIFT-SDXL	non-LLM	+0.324	+0.502
8	DINO-I	non-LLM	+0.311	+0.514
9	AM-RADIO C-RADIOv4-SO400M	non-LLM	+0.226	+0.541
10	CLIP-I	non-LLM	+0.135	+0.533

Table 2: Concept Preservation on ORIDa. Real-photo identity discrimination across 50 subjects \times 10 backgrounds: 2,250 within-subject cross-environment pairs and 2,250 random cross-subject pairs. AUC(within > cross) is the probability a random within-subject pair scores higher than a random cross-subject pair. **Bold**: ours — the first non-LLM CP metric to beat GPT-4o on a CP benchmark.

Metric	mean within	mean cross	Δ_{norm}	AUC
MaSC	0.740 \pm 0.071	0.402 \pm 0.064	+0.513	0.992
GPT-4o*	0.875 \pm 0.242	0.025 \pm 0.094	+0.850	0.986
AM-RADIO C-RADIOv4-SO400M	0.775 \pm 0.124	0.496 \pm 0.081	+0.416	0.961
SigLIP2 SO400M-NaFlex global pool	0.795 \pm 0.092	0.597 \pm 0.071	+0.318	0.954
DINOv3	0.553 \pm 0.230	0.134 \pm 0.113	+0.394	0.942
DreamSim	0.521 \pm 0.169	0.308 \pm 0.093	+0.241	0.873
DINO-I	0.495 \pm 0.201	0.245 \pm 0.141	+0.238	0.848
DIFT-SDXL	0.737 \pm 0.063	0.652 \pm 0.062	+0.174	0.834
CLIP-I	0.773 \pm 0.085	0.678 \pm 0.074	+0.167	0.800

*GPT-4o ratings rescaled from the native 0–4 rubric to $[0, 1]$ (raw / 4) for cross-metric comparability. AUC is invariant under monotonic transformations.

Same-backbone ablation. The same-backbone ablation establishes the contribution of the masked-maxcos aggregator as $\Delta\alpha = 0.102$: applying a global pool to the exact same SigLIP2 SO400M-NaFlex checkpoint yields $\alpha = +0.369$, confirming that the performance lift is driven purely by the aggregation strategy. Furthermore, while modern DINOv3 improves upon the standard DINO-I baseline ($\Delta\alpha = +0.034$), and DIFT-SDXL under its canonical recipe (timestep 261, `up_ft_index=1`, null prompt) achieves $\alpha = +0.324$, both still trail MaSC by a margin exceeding 0.125α .

Architectural ablation at matched parameter budget. We also compare against the two strongest architectural competitors in the modern non-LLM lineup: DreamSim (a NIGHTS-finetuned perceptual ensemble) and AM-RADIO C-RADIOv4-SO400M (which distills SigLIP2-g, DINOv3-7B, and SAM3 into a 431M ViT, matching our parameter budget and patch size). Both models underperform MaSC by $\Delta\alpha = 0.050$ and $\Delta\alpha = 0.245$, respectively.

4.2 CP on ORIDa

Table 2 reports CP on ORIDa (train subset), a real-photo identity-discrimination benchmark containing ground-truth per-object segmentation masks. We sample 50 subjects across 10 backgrounds using 1 photo per combination (specifically, the alphabetically first camera angle and first factual placement). From this, we form $50 \times \binom{10}{2} = 2,250$ within-subject cross-environment pairs and 2,250 random cross-subject pairs. Because ORIDa lacks human ratings, we evaluate performance using the Area Under the Curve (AUC), representing the probability that a within-subject pair outscores a cross-subject pair: $\text{AUC}(\text{within-pair} > \text{cross-pair})$. Figure 2 visualizes the corresponding score distributions.

MaSC is the first non-LLM metric to outperform GPT-4o on a CP benchmark ($\Delta \text{AUC} = 0.006$); this ranking inverts compared to DreamBench++ (where GPT-4o leads by $\Delta\alpha = 0.028$) as test conditions become more naturalistic. The underlying mechanism is visualized in Figure 2: continuous-cosine

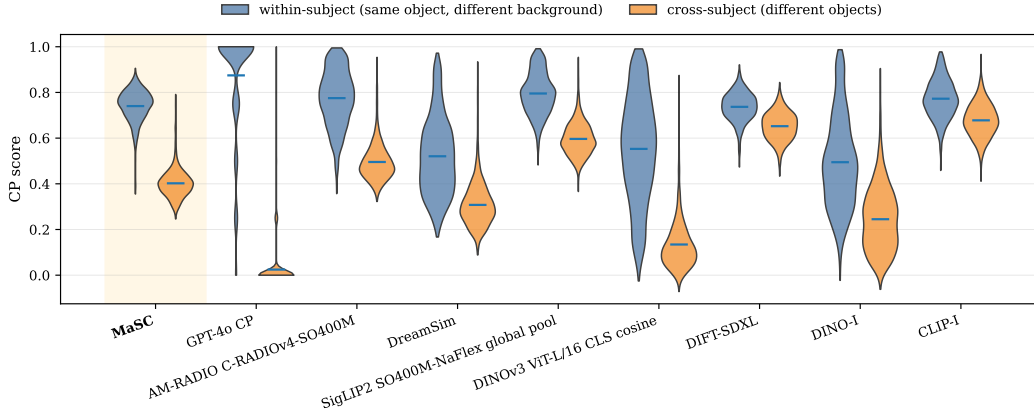


Figure 2: **ORIDa CP score distributions per metric:** within-subject pairs vs. cross-subject pairs; short horizontal lines mark the mean. Our proposed metric (MaSC) is highlighted with a shaded background. This figure visualizes the tail-overlap behavior that drives the AUC rankings in Table 2. Continuous-cosine metrics separate the two distributions cleanly, whereas the integer-rubric of GPT-4o yields the largest mean separation but heavily quantizes scores at rubric ties.

Table 3: Prompt Following on DreamBench++. Krippendorff α and Spearman ρ against pooled human PF ratings on the 6,607-key style-excluded subset. **Bold:** ours — a free byproduct of the CP forward pass that beats CLIP-T on the same backbone by $\Delta\alpha = +0.027$. We do not claim PF SOTA; VQAScore and ImageReward lead the non-LLM lineup.

#	Scorer	Kind	α	ρ
—	<i>Human inter-rater</i>	<i>ceiling</i>	+0.563	+0.571
1	GPT-4o	LLM judge	+0.547	+0.656
2	VQAScore	non-LLM	+0.504	+0.640
3	GPT-4V	LLM judge	+0.485	+0.661
4	ImageReward	non-LLM	+0.441	+0.611
5	MaSC	non-LLM	+0.354	+0.538
6	CLIP-T	non-LLM	+0.327	+0.477
7	SigLIP2 SO400M-NaFlex global pool	non-LLM	+0.326	+0.466
8	HPSv3	non-LLM	+0.299	+0.434

metrics cleanly separate the tails of the within- versus cross-subject distributions. In contrast, GPT-4o’s discrete 0–4 rubric quantizes scores, inducing heavy ties. Consequently, while its mean separation is the largest evaluated, its AUC ceiling is artificially capped because numerous cross-subject pairs score at or above the minimum within-subject score. The same-backbone ablation extends to real-world photos: the global pool yields an AUC of 0.954, whereas masked-maxcos achieves 0.992. This $\Delta \text{AUC} = 0.038$ improvement is smaller in absolute magnitude than the $\Delta\alpha = 0.102$ observed on DreamBench++, but consistent in direction. Notably, AM-RADIO outperforms DreamSim on ORIDa (reversing their DreamBench++ ranking), which aligns with AM-RADIO’s distillation training successfully capturing real-world object semantics; conversely, DreamSim’s NIGHTS-triplet fine-tuning transfers poorly to natural environment variations. DIFT-SDXL under its canonical recipe struggles again, yielding an AUC of 0.834 (ranking penultimate). Ultimately, MaSC is the only metric to achieve top performance across both evaluation regimes.

4.3 PF on DreamBench++

Table 3 reports PF α and ρ on the 6,607-key style-excluded DB++ subset. Style subjects are excluded because their prompts describe a visual style rather than a scene; consequently, subject-stripping these prompts produces grammatically malformed fragments.

MaSC’s PF score is derived at no additional vision-encoder cost from the CP forward pass, yet it outperforms CLIP-T on the same backbone by $\Delta\alpha = 0.027$. This improvement stems entirely from the structural intervention rather than the encoder: the same-backbone control (applying a SigLIP2

Table 4: Prompt Following ablation on the SigLIP2 SO400M-NaFlex backbone: image-side pooling ($\{\text{full, BG, FG}\}$) \times prompt-side subject stripping. Pooled Krippendorff α (Kd_o) against pooled DB++ human PF on the shared 6,607-key subset (style excluded). The **BG-pool** \times **strip** cell is **MaSC** (Tab. 3). The **FG-pool** control aligns with Sec. 4.3: pooling *onto* the subject collapses the signal ($\alpha < 0$). **FG-pool** \times **subject-stripped** is omitted (—) as evaluating isolated subjects against background-only text is structurally invalid.

Pool \ Prompt	full prompt α	subject-stripped α
BG-pool (MaSC)	+0.344	+0.354
Full pool (no mask)	+0.326	+0.348
FG-pool (inverse-mask control)	-0.108	—

global pool with the unstripped prompt) achieves $\alpha = +0.326$, essentially tied with CLIP-T’s $+0.327$. Swapping the backbone from CLIP to SigLIP2 yields no meaningful improvement for PF. While MaSC does not establish a new state-of-the-art for PF, its primary contribution is architectural efficiency. Currently, VQAScore ($+0.504$) and ImageReward ($+0.441$) lead the non-LLM lineup, outperforming MaSC by margins of $\Delta\alpha = 0.150$ and 0.087 , respectively. For a deployment already running SigLIP2 for CP, MaSC provides a PF score superior to CLIP-T without an additional vision-encoder forward pass. Furthermore, the foreground-pooled control on the same backbone drops to $\alpha = -0.108$ (Table 4). Pooling strictly *onto* the subject inverts the signal, validating the background-masking intervention and confirming that information isolated within the foreground actively degrades PF evaluation.

4.4 Aggregator Dominates Features

Holding the feature representation fixed, substituting our masked-maxcos aggregator with a mutual-NN foreground-recall aggregator (fraction of mutual NN matches that stay foreground-to-foreground) reduces α by 0.462 on SigLIP2 patch features and by 0.716 on DINOv3 patch features. As established in Section 3.2, the strict one-to-one constraint of mutual-NN severely over-penalizes the partial-preservation regime typical of generated outputs. By contrast, the performance gap between SigLIP2 and DINOv3 *under a fixed aggregator* is comparatively minor ($\Delta\alpha = 0.126$).

We also wired the same masked-maxcos aggregator into four specialized correspondence matchers (LoFTR [27], RoMa [4], MAST3R [9], SuperPoint+LightGlue [13]); all four land α -negative on DB++. This demonstrates that the aggregator cannot succeed in isolation; it requires underlying features that natively capture concept identity.

4.5 Compute and Runtime

Table 5 reports per-pair inference latency on a single NVIDIA GeForce RTX 3090 (24GB, driver 550.54.15, CUDA 12.4) paired with an AMD EPYC 7452 (32-core, 128 logical CPUs), running Ubuntu 22.04 with PyTorch 2.6.0 and cuDNN 9.1.0. Timings use fp32, bf16 where the canonical recipe uses it, are taken as the median over 20 timed calls after 5 warmups, and exclude image and mask IO. Mask extraction runs once per image and is cached, so it is not on the per-pair scoring path.

MaSC’s CP path requires 161 ms per pair, while PF requires 91 ms. A combined CP and PF deployment requires approximately 190–200 ms per pair; because reference features are cached across all prompts and seeds, the amortized cost is even lower. The lightweight encoder baselines (DINO-I, CLIP-I, DINOv3) are 3–5 \times faster but underperform by margins of $\Delta\alpha \geq 0.126$ on DreamBench++ CP. AM-RADIO, at 72 ms, is the fastest peer at a comparable parameter budget, yet it underperforms by $\Delta\alpha = 0.245$ on DreamBench++ and $\Delta \text{AUC} = 0.031$ on ORIDA. DIFT-SDXL is the slowest metric evaluated, requiring 1,400 ms ($\sim 9\times$ MaSC) while achieving only $\alpha = +0.324$. This suggests that relying on a diffusion backbone introduces substantial computational cost without corresponding performance gains in this setting. The 0.102α and 0.038 AUC improvements from the masked-maxcos aggregator introduce zero additional latency: both run at ~ 161 ms because the dominant cost is the shared SigLIP2 forward pass. On the PF side, although CLIP-T (17 ms) and ImageReward (36 ms) are faster, MaSC’s PF (91 ms) directly reuses the CP vision features. Compared to other high-performing PF metrics, MaSC is significantly more efficient; VQAScore (265 ms) and HPSv3 (301 ms) are approximately $3\times$ slower than MaSC while requiring significantly larger parameter budgets.

Table 5: Inference cost. Per-pair latency on a single RTX 3090, sorted by latency. Single fixed DB++ pair (object_00_motorcycle, dreambooth_sd seed 0, prompt 0, 512×512 inputs). Each metric is timed in its own subprocess with `torch.cuda.synchronize()` around every timed call. **Bold:** ours.

Metric	Table	Params (M)	Latency (ms / pair)
CLIP-T	PF	151	17.0
DINO-I	CP	22	31.8
ImageReward	PF	447	35.9
CLIP-I	CP	151	36.5
DINOv3 ViT-L/16 CLS cosine	CP	303	47.3
DreamSim	CP	266	60.0
AM-RADIO C-RADIOv4-SO400M	CP	431	71.8
SigLIP2 SO400M-NaFlex global pool	PF	1 136	89.4
MaSC	PF	1 136	91.3
MaSC	CP	428	160.7
SigLIP2 SO400M-NaFlex global pool	CP	1 136	161.4
VQAScore	PF	11 460	264.7
HPSv3	PF	8 292	300.9
DIFT-SDXL	CP	2 651	1 399.7
GPT-4o (API)	—	n/a	—

5 Discussion

The main finding is that personalization evaluation benefits more from spatially correct aggregation than from another unmasked global embedding: global image similarity mixes subject identity and scene content, whereas concept preservation and prompt following require different evidence. MaSC enforces this distinction by measuring identity from foreground reference patches with masked-maxcos and measuring scene adherence from a background-only embedding compared with a subject-stripped prompt, which explains why the same SigLIP2 backbone improves when global pooling is replaced by region-conditioned aggregation. The CP results support foreground-local evidence as the proper unit for subject fidelity: MaSC reaches $\alpha = +0.471$ on DreamBench++, outperforming all tested non-LLM baselines and GPT-4V while remaining only $\Delta\alpha = 0.028$ below GPT-4o, and reaches $AUC = 0.992$ on ORIDa, outperforming GPT-4o under the evaluated real-photo discrimination protocol. Same-backbone ablations show that the gain comes from masked aggregation rather than encoder choice alone, with improvements of $\Delta\alpha = +0.102$ on DreamBench++ and $\Delta AUC = +0.038$ on ORIDa, although the failed correspondence-matcher controls show that the aggregator still requires identity-aware features. The PF branch should be read more narrowly: background pooling with subject stripping improves over CLIP-T while reusing the CP visual features, but it does not surpass dedicated reward models such as VQAScore or ImageReward; its contribution is efficiency and diagnostic separation rather than PF state of the art. MaSC also has practical limits: it depends on externally supplied masks (though Appendix 6.1 demonstrates that performance remains highly robust across different modern segmentation architectures), mask failures affect both filtering and scores, near-empty-mask filtering changes the evaluated population, subject-name stripping is unsuitable for some style prompts, ORIDa lacks human ratings, and the method is designed for single-concept personalization rather than general aesthetic, compositional, or preference evaluation.

6 Conclusion

We introduced MaSC, a masked similarity metric for concept-driven text-to-image evaluation. Rather than relying on global image embeddings that conflate subject identity with scene content, MaSC spatially decomposes the image: foreground-reference patch matching measures concept preservation, while background-only text-image alignment measures prompt following, both from a shared frozen SigLIP2 forward pass. Across DreamBench++ and ORIDa, MaSC shows that aggregation matters as much as, or more than, encoder choice. It achieves the strongest non-LLM concept-preservation performance on DreamBench++, surpassing GPT-4V and approaching GPT-4o, and nearly perfectly separates same-subject from cross-subject pairs on ORIDa. Its prompt-following score also improves over CLIP-T without an additional vision-encoder pass. MaSC’s main limitation is its dependence on externally supplied foreground masks, which can introduce errors when segmentation fails or subjects are small, absent, or ambiguous. Future work should address mask uncertainty, multi-subject

settings, and broader personalization regimes. Overall, our results suggest that spatial attribution should be a central design principle for evaluating generative models.

Acknowledgments and Disclosure of Funding

Use unnumbered first level headings for the acknowledgments. All acknowledgments go at the end of the paper before the list of references. Moreover, you are required to declare funding (financial activities supporting the submitted work) and competing interests (related financial activities outside the submitted work). More information about this disclosure can be found at: <https://neurips.cc/Conferences/2026/PaperInformation/FundingDisclosure>.

Do **not** include this section in the anonymized submission, only in the final paper. You can use the `ack` environment provided in the style file to automatically hide this section in the anonymized submission.

References

- [1] Nicolas Carion, Laura Gustafson, Yuan-Ting Hu, Shoubhik Debnath, Ronghang Hu, Didac Suris, Chaitanya Ryali, Kalyan Vasudev Alwala, Haitham Khedr, Andrew Huang, Jie Lei, Tengyu Ma, Baishan Guo, Arpit Kalla, Markus Marks, Joseph Greer, Meng Wang, Peize Sun, Roman Rädle, Triantafyllos Afouras, Effrosyni Mavroudi, Katherine Xu, Tsung-Han Wu, Yu Zhou, Liliane Momeni, Rishi Hazra, Shuangrui Ding, Sagar Vaze, Francois Porcher, Feng Li, Siyuan Li, Aishwarya Kamath, Ho Kei Cheng, Piotr Dollár, Nikhila Ravi, Kate Saenko, Pengchuan Zhang, and Christoph Feichtenhofer. Sam 3: Segment anything with concepts, 2025.
- [2] Mathilde Caron, Hugo Touvron, Ishan Misra, Hervé Jegou, Julien Mairal, Piotr Bojanowski, and Armand Joulin. Emerging properties in self-supervised vision transformers. In *2021 IEEE/CVF International Conference on Computer Vision (ICCV)*, pages 9630–9640, 2021.
- [3] Daniel DeTone, Tomasz Malisiewicz, and Andrew Rabinovich. Superpoint: Self-supervised interest point detection and description, 2018.
- [4] Johan Edstedt, Qiyu Sun, Georg Bökman, Mårten Wadenbäck, and Michael Felsberg. Roma: Robust dense feature matching. In *2024 IEEE/CVF Conference on Computer Vision and Pattern Recognition (CVPR)*, page 19790–19800. IEEE, 2024.
- [5] Stephanie Fu, Netanel Tamir, Shobhita Sundaram, Lucy Chai, Richard Zhang, Tali Dekel, and Phillip Isola. Dreamsim: Learning new dimensions of human visual similarity using synthetic data. In *Advances in Neural Information Processing Systems*, volume 36, pages 50742–50768, 2023.
- [6] Rinon Gal, Yuval Alaluf, Yuval Atzmon, Or Patashnik, Amit H. Bermano, Gal Chechik, and Daniel Cohen-Or. An image is worth one word: Personalizing text-to-image generation using textual inversion, 2022.
- [7] Jinwoo Kim, Sangmin Han, Jinho Jeong, Jiwoo Choi, Dongyeoung Kim, and Seon Joo Kim. Orida: Object-centric real-world image composition dataset. In *Proceedings of the Computer Vision and Pattern Recognition Conference*, pages 3051–3060, 2025.
- [8] klaus krippendorff. Computing krippendorff’s alpha-reliability. 01 2011.
- [9] Vincent Leroy, Yohann Cabon, and Jérôme Revaud. Grounding image matching in 3d with mast3r, 2024.
- [10] Dongxu Li, Junnan Li, and Steven CH Hoi. Blip-diffusion: Pre-trained subject representation for controllable text-to-image generation and editing. *arXiv preprint arXiv:2305.14720*, 2023.
- [11] Junnan Li, Dongxu Li, Caoming Xiong, and Steven Hoi. Blip: Bootstrapping language-image pre-training for unified vision-language understanding and generation, 2022.
- [12] Zhiqiu Lin, Deepak Pathak, Baiqi Li, Jiayao Li, Xide Xia, Graham Neubig, Pengchuan Zhang, and Deva Ramanan. Evaluating text-to-visual generation with image-to-text generation. *arXiv preprint arXiv:2404.01291*, 2024.

- [13] Philipp Lindenberger, Paul-Edouard Sarlin, and Marc Pollefeys. Lightglue: Local feature matching at light speed, 2023.
- [14] Timo Lüddecke and Alexander Ecker. Image segmentation using text and image prompts. In *Proceedings of the IEEE/CVF Conference on Computer Vision and Pattern Recognition (CVPR)*, pages 7086–7096, June 2022.
- [15] Yuhang Ma, Xiaoshi Wu, Keqiang Sun, and Hongsheng Li. Hpsv3: Towards wide-spectrum human preference score, 2025.
- [16] Matthias Minderer, Alexey Gritsenko, Austin Stone, Maxim Neumann, Dirk Weissenborn, Alexey Dosovitskiy, Aravindh Mahendran, Anurag Arnab, Mostafa Dehghani, Zirui Shen, et al. Scaling open-vocabulary object detection. In *Advances in Neural Information Processing Systems*, volume 36, 2023.
- [17] OpenAI, :, Aaron Hurst, Adam Lerer, Adam P. Goucher, Adam Perelman, Aditya Ramesh, Aidan Clark, AJ Ostrow, Akila Welihinda, Alan Hayes, Alec Radford, Aleksander Mądry, Alex Baker-Whitcomb, Alex Beutel, Alex Borzunov, Alex Carney, Alex Chow, Alex Kirillov, Alex Nichol, Alex Paino, Alex Renzin, Alex Tachard Passos, Alexander Kirillov, Alexi Christakis, Alexis Conneau, Ali Kamali, Allan Jabri, Allison Moyer, Allison Tam, Amadou Crookes, Amin Tootoochian, Amin Tootoonchian, Ananya Kumar, Andrea Vallone, Andrej Karpathy, Andrew Braunstein, Andrew Cann, Andrew Codispoti, Andrew Galu, Andrew Kondrich, Andrew Tulloch, Andrey Mishchenko, Angela Baek, Angela Jiang, Antoine Pelisse, Antonia Woodford, Anuj Gosalia, Arka Dhar, Ashley Pantuliano, Avi Nayak, Avital Oliver, Barret Zoph, Behrooz Ghorbani, Ben Leimberger, Ben Rossen, Ben Sokolowsky, Ben Wang, Benjamin Zweig, Beth Hoover, Blake Samic, Bob McGrew, Bobby Spero, Bogo Giertler, Bowen Cheng, Brad Lightcap, Brandon Walkin, Brendan Quinn, Brian Guarraci, Brian Hsu, Bright Kellogg, Brydon Eastman, Camillo Lugaresi, Carroll Wainwright, Cary Bassin, Cary Hudson, Casey Chu, Chad Nelson, Chak Li, Chan Jun Shern, Channing Conger, Charlotte Barette, Chelsea Voss, Chen Ding, Cheng Lu, Chong Zhang, Chris Beaumont, Chris Hallacy, Chris Koch, Christian Gibson, Christina Kim, Christine Choi, Christine McLeavey, Christopher Hesse, Claudia Fischer, Clemens Winter, Coley Czarnecki, Colin Jarvis, Colin Wei, Constantin Koumouzelis, Dane Sherburn, Daniel Kappler, Daniel Levin, Daniel Levy, David Carr, David Farhi, David Mely, David Robinson, David Sasaki, Denny Jin, Dev Valladares, Dimitris Tsipras, Doug Li, Duc Phong Nguyen, Duncan Findlay, Edede Oiwoh, Edmund Wong, Ehsan Asdar, Elizabeth Proehl, Elizabeth Yang, Eric Antonow, Eric Kramer, Eric Peterson, Eric Sigler, Eric Wallace, Eugene Brevdo, Evan Mays, Farzad Khorasani, Felipe Petroski Such, Filippo Raso, Francis Zhang, Fred von Lohmann, Freddie Sulit, Gabriel Goh, Gene Oden, Geoff Salmon, Giulio Starace, Greg Brockman, Hadi Salman, Haiming Bao, Haitang Hu, Hannah Wong, Haoyu Wang, Heather Schmidt, Heather Whitney, Heewoo Jun, Hendrik Kirchner, Henrique Ponde de Oliveira Pinto, Hongyu Ren, Huiwen Chang, Hyung Won Chung, Ian Kivlichan, Ian O’Connell, Ian O’Connell, Ian Osband, Ian Silber, Ian Sohl, Ibrahim Okuyucu, Ikai Lan, Ilya Kostrikov, Ilya Sutskever, Ingmar Kanitscheider, Ishaan Gulrajani, Jacob Coxon, Jacob Menick, Jakub Pachocki, James Aung, James Betker, James Crooks, James Lennon, Jamie Kiros, Jan Leike, Jane Park, Jason Kwon, Jason Phang, Jason Teplitz, Jason Wei, Jason Wolfe, Jay Chen, Jeff Harris, Jenia Varavva, Jessica Gan Lee, Jessica Shieh, Ji Lin, Jiahui Yu, Jiayi Weng, Jie Tang, Jieqi Yu, Joanne Jang, Joaquin Quinonero Candela, Joe Beutler, Joe Landers, Joel Parish, Johannes Heidecke, John Schulman, Jonathan Lachman, Jonathan McKay, Jonathan Uesato, Jonathan Ward, Jong Wook Kim, Joost Huizinga, Jordan Sitkin, Jos Kraaijeveld, Josh Gross, Josh Kaplan, Josh Snyder, Joshua Achiam, Joy Jiao, Joyce Lee, Juntang Zhuang, Justyn Harriman, Kai Fricke, Kai Hayashi, Karan Singhal, Katy Shi, Kavın Karthik, Kayla Wood, Kendra Rimbach, Kenny Hsu, Kenny Nguyen, Keren Gu-Lemberg, Kevin Button, Kevin Liu, Kiel Howe, Krithika Muthukumar, Kyle Luther, Lama Ahmad, Larry Kai, Lauren Itow, Lauren Workman, Leher Pathak, Leo Chen, Li Jing, Lia Guy, Liam Fedus, Liang Zhou, Lien Mamitsuka, Lilian Weng, Lindsay McCallum, Lindsey Held, Long Ouyang, Louis Feuvrier, Lu Zhang, Lukas Kondraciuk, Lukasz Kaiser, Luke Hewitt, Luke Metz, Lyric Doshi, Mada Aflak, Maddie Simens, Madelaine Boyd, Madeleine Thompson, Marat Dukhan, Mark Chen, Mark Gray, Mark Hudnall, Marvin Zhang, Marwan Aljubeih, Mateusz Litwin, Matthew Zeng, Max Johnson, Maya Shetty, Mayank Gupta, Meghan Shah, Mehmet Yatbaz, Meng Jia Yang, Mengchao Zhong, Mia Glaese, Mianna Chen, Michael Janner, Michael Lampe, Michael Petrov, Michael Wu, Michele Wang, Michelle Fradin, Michelle Pokrass, Miguel Castro,

Miguel Oom Temudo de Castro, Mikhail Pavlov, Miles Brundage, Miles Wang, Minal Khan, Mira Murati, Mo Bavarian, Molly Lin, Murat Yesildal, Nacho Soto, Natalia Gimelshein, Natalie Cone, Natalie Staudacher, Natalie Summers, Natan LaFontaine, Neil Chowdhury, Nick Ryder, Nick Stathas, Nick Turley, Nik Tezak, Niko Felix, Nithanth Kudige, Nitish Keskar, Noah Deutsch, Noel Bundick, Nora Puckett, Ofir Nachum, Ola Okelola, Oleg Boiko, Oleg Murk, Oliver Jaffe, Olivia Watkins, Olivier Godement, Owen Campbell-Moore, Patrick Chao, Paul McMillan, Pavel Belov, Peng Su, Peter Bak, Peter Bakkum, Peter Deng, Peter Dolan, Peter Hoeschele, Peter Welinder, Phil Tillet, Philip Pronin, Philippe Tillet, Prafulla Dhariwal, Qiming Yuan, Rachel Dias, Rachel Lim, Rahul Arora, Rajan Troll, Randall Lin, Rapha Gontijo Lopes, Raul Puri, Reah Miyara, Reimar Leike, Renaud Gaubert, Reza Zamani, Ricky Wang, Rob Donnelly, Rob Honsby, Rocky Smith, Rohan Sahai, Rohit Ramchandani, Romain Huet, Rory Carmichael, Rowan Zellers, Roy Chen, Ruby Chen, Ruslan Nigmatullin, Ryan Cheu, Saachi Jain, Sam Altman, Sam Schoenholz, Sam Toizer, Samuel Miserendino, Sandhini Agarwal, Sara Culver, Scott Ethersmith, Scott Gray, Sean Grove, Sean Metzger, Shamez Hermani, Shantanu Jain, Shengjia Zhao, Sherwin Wu, Shino Jomoto, Shirong Wu, Shuaiqi, Xia, Sonia Phene, Spencer Papay, Srinivas Narayanan, Steve Coffey, Steve Lee, Stewart Hall, Suchir Balaji, Tal Broda, Tal Stramer, Tao Xu, Tarun Gogineni, Taya Christianson, Ted Sanders, Tejal Patwardhan, Thomas Cunningham, Thomas Degry, Thomas Dimson, Thomas Raoux, Thomas Shadwell, Tianhao Zheng, Todd Underwood, Todor Markov, Toki Sherbakov, Tom Rubin, Tom Stasi, Tomer Kaftan, Tristan Heywood, Troy Peterson, Tyce Walters, Tyna Eloundou, Valerie Qi, Veit Moeller, Vinnie Monaco, Vishal Kuo, Vlad Fomenko, Wayne Chang, Weiyi Zheng, Wenda Zhou, Wesam Manassra, Will Sheu, Wojciech Zaremba, Yash Patil, Yilei Qian, Yongjik Kim, Youlong Cheng, Yu Zhang, Yuchen He, Yuchen Zhang, Yujia Jin, Yunxing Dai, and Yury Malkov. Gpt-4o system card, 2024.

- [18] OpenAI, Josh Achiam, Steven Adler, Sandhini Agarwal, Lama Ahmad, Ilge Akkaya, Florencia Leoni Aleman, Diogo Almeida, Janko Altmenschmidt, Sam Altman, Shyamal Anadkat, Red Avila, Igor Babuschkin, Suchir Balaji, Valerie Balcom, Paul Baltescu, Haiming Bao, Mohammad Bavarian, Jeff Belgum, Irwan Bello, Jake Berdine, Gabriel Bernadett-Shapiro, Christopher Berner, Lenny Bogdonoff, Oleg Boiko, Madelaine Boyd, Anna-Luisa Brakman, Greg Brockman, Tim Brooks, Miles Brundage, Kevin Button, Trevor Cai, Rosie Campbell, Andrew Cann, Brittany Carey, Chelsea Carlson, Rory Carmichael, Brooke Chan, Che Chang, Fotis Chantzis, Derek Chen, Sully Chen, Ruby Chen, Jason Chen, Mark Chen, Ben Chess, Chester Cho, Casey Chu, Hyung Won Chung, Dave Cummings, Jeremiah Currier, Yunxing Dai, Cory Decareaux, Thomas Degry, Noah Deutsch, Damien Deville, Arka Dhar, David Dohan, Steve Dowling, Sheila Dunning, Adrien Ecoffet, Atty Eleti, Tyna Eloundou, David Farhi, Liam Fedus, Niko Felix, Simón Posada Fishman, Juston Forte, Isabella Fulford, Leo Gao, Elie Georges, Christian Gibson, Vik Goel, Tarun Gogineni, Gabriel Goh, Rapha Gontijo-Lopes, Jonathan Gordon, Morgan Grafstein, Scott Gray, Ryan Greene, Joshua Gross, Shixiang Shane Gu, Yufei Guo, Chris Hallacy, Jesse Han, Jeff Harris, Yuchen He, Mike Heaton, Johannes Heidecke, Chris Hesse, Alan Hickey, Wade Hickey, Peter Hoeschele, Brandon Houghton, Kenny Hsu, Shengli Hu, Xin Hu, Joost Huizinga, Shantanu Jain, Shawn Jain, Joanne Jang, Angela Jiang, Roger Jiang, Haozhun Jin, Denny Jin, Shino Jomoto, Billie Jonn, Heewoo Jun, Tomer Kaftan, Łukasz Kaiser, Ali Kamali, Ingmar Kanitscheider, Nitish Shirish Keskar, Tabarak Khan, Logan Kilpatrick, Jong Wook Kim, Christina Kim, Yongjik Kim, Jan Hendrik Kirchner, Jamie Kiros, Matt Knight, Daniel Kokotajlo, Łukasz Kondraciuk, Andrew Kondrich, Aris Konstantinidis, Kyle Kopic, Gretchen Krueger, Vishal Kuo, Michael Lampe, Ikai Lan, Teddy Lee, Jan Leike, Jade Leung, Daniel Levy, Chak Ming Li, Rachel Lim, Molly Lin, Stephanie Lin, Mateusz Litwin, Theresa Lopez, Ryan Lowe, Patricia Lue, Anna Makanju, Kim Malfacini, Sam Manning, Todor Markov, Yaniv Markovski, Bianca Martin, Katie Mayer, Andrew Mayne, Bob McGrew, Scott Mayer McKinney, Christine McLeavey, Paul McMillan, Jake McNeil, David Medina, Aalok Mehta, Jacob Menick, Luke Metz, Andrey Mishchenko, Pamela Mishkin, Vinnie Monaco, Evan Morikawa, Daniel Mossing, Tong Mu, Mira Murati, Oleg Murk, David Mély, Ashvin Nair, Reiichiro Nakano, Rajeesh Nayak, Arvind Neelakantan, Richard Ngo, Hyeonwoo Noh, Long Ouyang, Cullen O’Keefe, Jakub Pachocki, Alex Paino, Joe Palermo, Ashley Pantuliano, Giambattista Parascandolo, Joel Parish, Emy Parparita, Alex Passos, Mikhail Pavlov, Andrew Peng, Adam Perelman, Filipe de Avila Belbute Peres, Michael Petrov, Henrique Ponde de Oliveira Pinto, Michael, Pokorny, Michelle Pokrass, Vitchyr H. Pong, Tolly Powell, Alethea Power, Boris Power, Elizabeth Proehl, Raul Puri, Alec Radford, Jack Rae, Aditya Ramesh,

Cameron Raymond, Francis Real, Kendra Rimbach, Carl Ross, Bob Rotsted, Henri Roussez, Nick Ryder, Mario Saltarelli, Ted Sanders, Shibani Santurkar, Girish Sastry, Heather Schmidt, David Schnurr, John Schulman, Daniel Selsam, Kyla Sheppard, Toki Sherbakov, Jessica Shieh, Sarah Shoker, Pranav Shyam, Szymon Sidor, Eric Sigler, Maddie Simens, Jordan Sitkin, Katarina Slama, Ian Sohl, Benjamin Sokolowsky, Yang Song, Natalie Staudacher, Felipe Petroski Such, Natalie Summers, Ilya Sutskever, Jie Tang, Nikolas Tezak, Madeleine B. Thompson, Phil Tillet, Amin Tootoonchian, Elizabeth Tseng, Preston Tuggle, Nick Turley, Jerry Tworek, Juan Felipe Cerón Uribe, Andrea Vallone, Arun Vijayvergiya, Chelsea Voss, Carroll Wainwright, Justin Jay Wang, Alvin Wang, Ben Wang, Jonathan Ward, Jason Wei, CJ Weinmann, Akila Welihinda, Peter Welinder, Jiayi Weng, Lillian Weng, Matt Wiethoff, Dave Willner, Clemens Winter, Samuel Wolrich, Hannah Wong, Lauren Workman, Sherwin Wu, Jeff Wu, Michael Wu, Kai Xiao, Tao Xu, Sarah Yoo, Kevin Yu, Qiming Yuan, Wojciech Zaremba, Rowan Zellers, Chong Zhang, Marvin Zhang, Shengjia Zhao, Tianhao Zheng, Juntang Zhuang, William Zhuk, and Barret Zoph. Gpt-4 technical report, 2024.

- [19] Yuang Peng, Yuxin Cui, Haomiao Tang, Zekun Qi, Runpei Dong, Jing Bai, Chunrui Han, Zheng Ge, Xiangyu Zhang, and Shu-Tao Xia. Dreambench++: A human-aligned benchmark for personalized image generation. In *The Thirteenth International Conference on Learning Representations*, 2025.
- [20] Alec Radford, Jong Wook Kim, Chris Hallacy, Aditya Ramesh, Gabriel Goh, Sandhini Agarwal, Girish Sastry, Amanda Askell, Pamela Mishkin, Jack Clark, Gretchen Krueger, and Ilya Sutskever. Learning transferable visual models from natural language supervision, 2021.
- [21] Mike Ranzinger, Greg Heinrich, Jan Kautz, and Pavlo Molchanov. Am-radio: Agglomerative vision foundation model reduce all domains into one. In *Proceedings of the IEEE/CVF Conference on Computer Vision and Pattern Recognition (CVPR)*, pages 12490–12500, June 2024.
- [22] Nikhila Ravi, Valentin Gabeur, Yuan-Ting Hu, Ronghang Hu, Chaitanya Ryali, Tengyu Ma, Haitham Khedr, Roman Rädle, Chloe Rolland, Laura Gustafson, Eric Mintun, Junting Pan, Kalyan Vasudev Alwala, Nicolas Carion, Chao-Yuan Wu, Ross Girshick, Piotr Dollár, and Christoph Feichtenhofer. Sam 2: Segment anything in images and videos. *arXiv preprint arXiv:2408.00714*, 2024.
- [23] Tianhe Ren, Shilong Liu, Ailing Zeng, Jing Lin, Kunchang Li, He Cao, Jiayu Chen, Xinyu Huang, Yukang Chen, Feng Yan, Zhaoyang Zeng, Hao Zhang, Feng Li, Jie Yang, Hongyang Li, Qing Jiang, and Lei Zhang. Grounded sam: Assembling open-world models for diverse visual tasks, 2024.
- [24] Robin Rombach, Andreas Blattmann, Dominik Lorenz, Patrick Esser, and Björn Ommer. High-resolution image synthesis with latent diffusion models, 2022.
- [25] Nataniel Ruiz, Yuanzhen Li, Varun Jampani, Yael Pritch, Michael Rubinstein, and Kfir Aberman. Dreambooth: Fine tuning text-to-image diffusion models for subject-driven generation. 2022.
- [26] Oriane Siméoni, Huy V. Vo, Maximilian Seitzer, Federico Baldassarre, Maxime Oquab, Cijo Jose, Vasil Khalidov, Marc Szafraniec, Seungeun Yi, Michaël Ramamonjisoa, Francisco Massa, Daniel Haziza, Luca Wehrstedt, Jianyuan Wang, Timothée Darcet, Théo Moutakanni, Leonel Sentana, Claire Roberts, Andrea Vedaldi, Jamie Tolan, John Brandt, Camille Couprie, Julien Mairal, Hervé Jégou, Patrick Labatut, and Piotr Bojanowski. DINOv3, 2025.
- [27] Jiaming Sun, Zehong Shen, Yuang Wang, Hujun Bao, and Xiaowei Zhou. LoFTR: Detector-free local feature matching with transformers. *CVPR*, 2021.
- [28] Quan Sun, Yufeng Cui, Xiaosong Zhang, Fan Zhang, Qiying Yu, Zhengxiong Luo, Yueze Wang, Yongming Rao, Jingjing Liu, Tiejun Huang, and Xinlong Wang. Generative multimodal models are in-context learners. 2023.
- [29] Luming Tang, Menglin Jia, Qianqian Wang, Cheng Perng Phoo, and Bharath Hariharan. Emergent correspondence from image diffusion. In *Thirty-seventh Conference on Neural Information Processing Systems*, 2023.

- [30] Michael Tschannen, Alexey Gritsenko, Xiao Wang, Muhammad Ferjad Naeem, Ibrahim Alabdulmohsin, Nikhil Parthasarathy, Talfan Evans, Lucas Beyer, Ye Xia, Basil Mustafa, Olivier Hénaff, Jeremiah Harmsen, Andreas Steiner, and Xiaohua Zhai. Siglip 2: Multilingual vision-language encoders with improved semantic understanding, localization, and dense features. *arXiv preprint arXiv:2502.14786*, 2025.
- [31] Peng Wang, Shuai Bai, Sinan Tan, Shijie Wang, Zhihao Fan, Jinze Bai, Keqin Chen, Xuejing Liu, Jialin Wang, Wenbin Ge, Yang Fan, Kai Dang, Mengfei Du, Xuancheng Ren, Rui Men, Dayiheng Liu, Chang Zhou, Jingren Zhou, and Junyang Lin. Qwen2-vl: Enhancing vision-language model’s perception of the world at any resolution, 2024.
- [32] Jiazheng Xu, Xiao Liu, Yuchen Wu, Yuxuan Tong, Qinkai Li, Ming Ding, Jie Tang, and Yuxiao Dong. Imagereward: learning and evaluating human preferences for text-to-image generation. In *Proceedings of the 37th International Conference on Neural Information Processing Systems*, pages 15903–15935, 2023.
- [33] Hu Ye, Jun Zhang, Sibio Liu, Xiao Han, and Wei Yang. Ip-adapter: Text compatible image prompt adapter for text-to-image diffusion models. 2023.

6.1 Sensitivity to Segmentation Source

To verify that MaSC’s performance is not artificially tied to the specific capabilities of SAM3, we conducted a sensitivity analysis across four distinct zero-shot segmentation pipelines: SAM3, CLIPSeg [14], Grounded-SAM2 [22, 23], and OWLv2 [16] + SAM2. We evaluated both the Concept Preservation (CP) and Prompt Following (PF) branches on strictly intersected subsets of DreamBench++ where all four extractors successfully produced a valid mask (5,315 keys for CP, and 4,998 style-excluded keys for PF).

As shown in Table 6, MaSC’s CP score performed consistently across all mask sources. The Krippendorff α varied by at most $\Delta\alpha = 0.012$, and Spearman ρ by at most $\Delta\rho = 0.002$. Notably, the lighter and older CLIPSeg architecture marginally outperformed the SAM3 baseline ($\alpha = +0.482$), demonstrating that our spatial decomposition strategy requires only general subject localization rather than pixel-perfect segmentation boundaries.

Similarly, the PF branch (Table 7) remained highly stable. Because the PF branch uses the mask to suppress foreground tokens, this result confirms that slight variations in segmentation boundaries do not meaningfully alter the background-pooled embedding. Together, these results confirm that MaSC’s improvement comes from the structural intervention of spatial decomposition, rather than the isolated accuracy of modern segmentation models.

Table 6: **CP Sensitivity to Segmentation Source.** Evaluated on a strictly intersected 5,315-key subset. The performance gaps ($\Delta\alpha$, $\Delta\rho$) are relative to the SAM3 baseline. Performance remains highly stable, with the lighter CLIPSeg architecture achieving the highest score.

Mask Source	α	$\Delta\alpha$	ρ	$\Delta\rho$
SAM3 (baseline)	+0.470	—	+0.627	—
CLIPSeg	+0.482	+0.012	+0.630	+0.002
Grounded-SAM2	+0.472	+0.002	+0.628	+0.001
OWLv2 + SAM2	+0.473	+0.003	+0.626	-0.001

Table 7: **PF Sensitivity to Segmentation Source.** Evaluated on a strictly intersected 4,998-key subset (style prompts excluded). The background-pooling PF metric is highly robust to mask variations, with maximum score fluctuations of just $\Delta\alpha = 0.005$.

Mask Source	α	$\Delta\alpha$	ρ	$\Delta\rho$
SAM3 (baseline)	+0.395	—	+0.555	—
CLIPSeg	+0.397	+0.002	+0.556	+0.001
Grounded-SAM2	+0.391	-0.004	+0.552	-0.003
OWLv2 + SAM2	+0.390	-0.005	+0.552	-0.004

Table 8: Dataset licenses and access terms. License information should be checked against the official dataset source before public release of any derived benchmark tables or redistributed files.

Dataset	License / terms	Notes for MaSC use
DreamBench++	Code: Apache 2.0 (https://github.com/yuangpeng/dreambench_plus); image and human rating data: released via Google Drive accompanying the paper, no explicit license stated	The 7,135-key CP subset and 6,607-key PF subset are derived from the DreamBench++ release. We use the image and rating data solely for academic evaluation, consistent with the paper’s stated purpose; no subject images or human ratings are redistributed by MaSC, only processed evaluation tables and per-key metric scores.
ORIDa	Dataset access via the authors’ download form (Yonsei University); no explicit dataset license is published on the project page. Paper text: CC BY-NC-SA 4.0.	The 50-subject \times 10-environment subset and the corresponding within-/cross-subject pair lists are constructed from ORIDa-train. Provided per-object segmentation masks are used as-is. We treat use as non-commercial academic research, consistent with the paper’s CC BY-NC-SA 4.0 release; no images, masks, or derivatives are redistributed by MaSC. The dataset is cited per the authors’ attribution requirement, and the exact access terms recorded at download time are preserved in the supplementary manifest.

N. Licenses, Access Terms, and Attribution

Dataset redistribution. The MaSC supplement does not redistribute third-party dataset images, masks, or human ratings unless explicitly allowed by the corresponding license. Instead, it provides scripts and metadata that reproduce the reported scores after the user obtains each dataset under its original terms.

Table 9: External model and metric assets used for MaSC and baselines. The exact implementation and checkpoint source are recorded in the supplementary manifest.

Asset	License / terms	Notes for MaSC use
SigLIP2 NaFlex [30]	SO400M- Apache 2.0 for the evaluated Google/Hugging Face release	Frozen vision-language backbone for MaSC. The exact checkpoint identifier is recorded in the manifest, and license notices are preserved.
SAM3 [1]	SAM License (Meta); non-exclusive, royalty-free research and commercial use with attribution; prohibited end uses include military or warfare, weapons, ITAR-controlled, nuclear, espionage, and reverse engineering	Concept-mask source on DreamBench++. The exact SAM3 checkpoint is recorded in the manifest, MaSC’s use is consistent with the SAM License, and the use of SAM Materials is acknowledged in the paper as required by the license.
CLIP [20]	MIT for the OpenAI repository code	Used as the CLIP-I appearance baseline and CLIP-T text-image baseline. The exact checkpoint/source is recorded in the manifest, and the MIT license notice is preserved.
DINO [2]	Apache 2.0 (Meta)	Used as the DINO-I baseline via the <code>dino_vits8</code> checkpoint shipped with DreamBench++. Copyright and license notices are preserved.
DINOv3 [26]	Meta DINOv3 license	Used as the modern self-supervised CP baseline. Use, redistribution, and derivatives must follow Meta’s DINOv3 license terms.
DreamSim [5]	MIT (https://github.com/ssundaram21/dreamsim)	NIGHTS-finetuned perceptual ensemble used as a CP baseline. License notices are preserved.
AM-RADIO C-RADIOv4-SO400M [21]	NVIDIA Open Model License Agreement (June 2024); permits commercial and non-commercial use with attribution	Distillation-trained ViT used as a matched-parameter-budget CP baseline. The exact checkpoint and license document are recorded in the manifest; the NVIDIA Open Model License terms are respected. (Note: the related RADIO and E-RADIO variants ship under the NVIDIA Source Code License-NC and are not used in this work.)
DIFT [29] (Stable Diffusion XL [24])	DIFT code: MIT; SDXL: CreativeML Open RAIL++-M	DIFT-SDXL canonical-recipe baseline (timestep 261, <code>up_ft_index=1</code> , null prompt). SDXL weights are used under Stability AI’s RAIL++-M terms; DIFT code license notices are preserved.
ImageReward [32]	Apache 2.0 (https://github.com/zai-org/ImageReward)	PF baseline. License notices are preserved.
VQAScore (clip-flant5-xxl) [12]	Apache 2.0 (https://github.com/linzhiqiu/t2v_metrics)	PF baseline. License notices are preserved.
HPSv3 (Qwen2-VL-7B-Instruct) [15, 31]	HPSv3 code: MIT; Qwen2-VL-7B-Instruct: Apache 2.0	PF baseline. The Qwen2-VL-7B-Instruct backbone is used under its Apache 2.0 license; HPSv3 code license notices are preserved. (The 72B variant of Qwen2-VL ships under the Tongyi Qianwen license and is not used in this work.)
LoFTR [27]	Apache 2.0	Used as a correspondence-matcher control in the aggregator analysis. Copyright and license notices are preserved.
RoMa [4]	MIT (https://github.com/Parskatt/RoMa); the bundled DINOv2 sub-component is Apache 2.0	Used as a correspondence-matcher control. License notices for both the MIT-licensed RoMa code and the Apache 2.0-licensed DINOv2 sub-component are preserved.
MASt3R [9]	CC BY-NC-SA 4.0; non-commercial use only	Used as a correspondence-matcher control. Non-commercial and ShareAlike restrictions are stated; commercial use may require separate permission.
LightGlue [13]	Apache 2.0	Used as part of the SuperPoint+LightGlue control. Code and pretrained weights are released under Apache 2.0.
SuperPoint [3]	MIT (https://github.com/rpautrat/SuperPoint)	Used as part of the SuperPoint+LightGlue control. The open MIT re-implementation by rpautrat is used (not the Magic Leap restrictive release); license notices are preserved.
GPT-4V / GPT-4o [18, 17]	OpenAI API; OpenAI Terms of Use	LLM-judge baselines. DreamBench++ scores are reused from the public release; ORIDA scores are obtained via the OpenAI API in accordance with OpenAI’s terms.
SAM 2 [22]	Apache 2.0 (Meta) for code and model checkpoints; the bundled <code>cc_torch</code> post-processing utility is BSD-3-Clause	Concept-mask source / segmentation control. The exact SAM 2 checkpoint is recorded in the manifest, and Apache 2.0 license notices are preserved.
Grounded SAM [23]	Apache 2.0 (https://github.com/IDEA-Research/Grounded-Segment-Anything); bundles Grounding DINO (Apache 2.0) and Segment Anything (see SAM/SAM 2 rows)	Open-vocabulary segmentation control. The Grounded SAM glue code is used under Apache 2.0; bundled component licenses are honored independently and recorded in the manifest.
CLIPSeg [14]	Source code: MIT (https://github.com/timoj1/clipseg); released weights (CIDAS/clipseg-rd64-refined on Hugging Face); Apache 2.0	Text-prompted segmentation control. The exact checkpoint is recorded in the manifest; both the MIT code license and the Apache 2.0 weights license are preserved.
OWLv2 [16]	Apache 2.0 (Google) for both code and model checkpoints	Open-vocabulary detection control. The exact checkpoint identifier is recorded in the manifest, and Apache 2.0 license notices are preserved.

NeurIPS Paper Checklist

1. Claims

Question: Do the main claims made in the abstract and introduction accurately reflect the paper’s contributions and scope?

Answer: [Yes]

Justification: The abstract and introduction state that MaSC is a unified concept-preservation and prompt-following metric that scores both signals from a single SigLIP2 forward pass given an externally supplied concept mask. The five claimed contributions — DreamBench++ CP performance, ORIDa identity discrimination, the same-backbone ablation, the matched-budget comparison, and the PF result — each correspond to a specific empirical evaluation reported in the paper. The scope is single-concept text-to-image personalization, and the paper explicitly does not claim PF state-of-the-art.

2. Limitations

Question: Does the paper discuss the limitations of the work performed by the authors?

Answer: [Yes]

Justification: The paper discusses its limitations in the Discussion and Conclusion: dependence on externally supplied foreground masks, the effect of mask-failure filtering on the evaluated population, the inapplicability of subject-name stripping to style prompts, the absence of human ratings on ORIDa, and the restriction to single-concept personalization. The Prompt Following section explicitly notes that MaSC does not establish PF state-of-the-art and is positioned as a free byproduct of the concept-preservation forward pass rather than a dedicated reward model.

3. Theory assumptions and proofs

Question: For each theoretical result, does the paper provide the full set of assumptions and a complete (and correct) proof?

Answer: [N/A]

Justification: The paper does not present formal theoretical results, theorems, or proofs. The mathematical content defines the masked-maxcos concept-preservation score, the background-pooled prompt-following score, and the subject-stripping operator used in the empirical evaluation.

4. Experimental result reproducibility

Question: Does the paper fully disclose all the information needed to reproduce the main experimental results of the paper to the extent that it affects the main claims and/or conclusions of the paper (regardless of whether the code and data are provided or not)?

Answer: [Yes]

Justification: The paper specifies the metric definitions, the frozen public SigLIP2 SO400M-NaFlex backbone, the mask source and filtering protocol, and the dataset-specific subject sampling for ORIDa. Comparator configurations — including the DIFT-SDXL canonical recipe, the DINOv3 and DreamSim variants, AM-RADIO, VQAScore, ImageReward, and HPSv3 — are documented in the related-work and results sections. Both evaluation datasets (DreamBench++ and ORIDa) are publicly available, and the paper announces release of a pip-installable Python package for the metric and comparator reproductions.

5. Open access to data and code

Question: Does the paper provide open access to the data and code, with sufficient instructions to faithfully reproduce the main experimental results, as described in supplemental material?

Answer: [Yes]

Justification: We provide anonymized supplementary code (<https://anonymous.4open.science/r/masc-reproduction-3536>) containing evaluation scripts to reproduce the MaSC scores, the same-backbone and aggregator ablations, and the reported correlations and AUCs against every comparator. The metric is also released as a pip-installable Python package (masc-metric). The raw datasets are existing public

benchmarks (DreamBench++ and ORIDa); the supplementary material describes how to obtain them and reproduce the processed evaluation tables.

6. Experimental setting/details

Question: Does the paper specify all the training and test details (e.g., data splits, hyperparameters, how they were chosen, type of optimizer) necessary to understand the results?

Answer: [Yes]

Justification: The paper is training-free; it specifies the frozen backbone, the mask source and filtering thresholds, the DreamBench++ subset sizes for CP and PF, and the ORIDa sampling protocol used for the within- and cross-subject pair construction. Comparator configurations — including the DIFT-SDXL canonical recipe, DINOv3 and DreamSim variants, AM-RADIO, VQAScore, ImageReward, and HPSv3 — are documented alongside the results, and the evaluation statistics are stated for each table.

7. Experiment statistical significance

Question: Does the paper report error bars suitably and correctly defined or other appropriate information about the statistical significance of the experiments?

Answer: [Yes]

Justification: The metric is deterministic, so there is no run-to-run variance to report. The headline numbers are computed over the full 7,135-key DreamBench++ apples-to-apples subset and the 4,500 ORIDa pairs; the ORIDa table additionally reports per-pair within- and cross-subject score distributions with standard deviations. A same-backbone ablation isolates the spatial decomposition from the encoder.

8. Experiments compute resources

Question: For each experiment, does the paper provide sufficient information on the computer resources (type of compute workers, memory, time of execution) needed to reproduce the experiments?

Answer: [Yes]

Justification: The runtime table reports per-pair latency in milliseconds and parameter counts for each evaluated metric. The hardware and software stack used for the benchmark is also specified, including the NVIDIA GeForce RTX 3090 GPU, CUDA version, AMD EPYC 7452 CPU, logical-CPU count, operating system, PyTorch, and cuDNN versions, along with the timing protocol (median over 20 calls after 5 warmups, image and mask IO excluded).

9. Code of ethics

Question: Does the research conducted in the paper conform, in every respect, with the NeurIPS Code of Ethics <https://neurips.cc/public/EthicsGuidelines>?

Answer: [Yes]

Justification: The research uses existing public personalization benchmarks and pretrained models for evaluating text-to-image personalization metrics, and does not involve human-subject experiments, private data collection, or deployment decisions. We have reviewed the NeurIPS Code of Ethics and believe the work conforms to it.

10. Broader impacts

Question: Does the paper discuss both potential positive societal impacts and negative societal impacts of the work performed?

Answer: [Yes]

Justification: The positive impact of MaSC is that it provides a fast, reproducible, non-API personalization metric, lowering the compute and cost barrier to rigorous benchmarking of personalization methods and reducing reliance on opaque LLM judges. Potential negative impacts include over-reliance on a proxy metric in deployment-critical settings, or its use to accelerate optimization of subject-driven generation models that can be misused for non-consensual or deceptive imagery; MaSC should therefore be used as a diagnostic evaluation tool rather than as a substitute for human review in sensitive applications.

11. Safeguards

Question: Does the paper describe safeguards that have been put in place for responsible release of data or models that have a high risk for misuse (e.g., pre-trained language models, image generators, or scraped datasets)?

Answer: [N/A]

Justification: The paper does not release high-risk generative models, pretrained language models, scraped datasets, or data intended for direct deployment in sensitive applications. The released assets are evaluation code, metric scripts, and a pip-installable package wrapping a frozen public SigLIP2 checkpoint.

12. Licenses for existing assets

Question: Are the creators or original owners of assets (e.g., code, data, models), used in the paper, properly credited and are the license and terms of use explicitly mentioned and properly respected?

Answer: [Yes]

Justification: The paper cites the original sources for all datasets, pretrained models, and metric implementations used in the evaluation. The supplementary material lists the license or access terms for each asset, including DreamBench++, ORIDa, SigLIP2, SAM3, DINO, DINOv3, DreamSim, AM-RADIO, DIFT/Stable Diffusion XL, CLIP, ImageReward, VQAScore, HPSv3, the correspondence-matcher controls (LoFTR, RoMa, MAST3R, LightGlue, SuperPoint), and the GPT-4V/4o API judges. The experiments are conducted in accordance with these terms, and raw third-party datasets, masks, and human ratings are not redistributed.

13. New assets

Question: Are new assets introduced in the paper well documented and is the documentation provided alongside the assets?

Answer: [Yes]

Justification: The paper introduces the MaSC evaluation code, comparator reproduction scripts, and the pip-installable masc-metric package. These assets are documented in the supplementary material, including expected inputs, mask-source assumptions, filtering thresholds, metric computation, comparator configurations, runtime assumptions, and known limitations.

14. Crowdsourcing and research with human subjects

Question: For crowdsourcing experiments and research with human subjects, does the paper include the full text of instructions given to participants and screenshots, if applicable, as well as details about compensation (if any)?

Answer: [N/A]

Justification: The paper does not involve crowdsourcing, user studies, annotation by human participants, or research with human subjects. All evaluations are performed on existing public benchmarks; the human ratings used as ground truth on DreamBench++ are obtained as-is from the original release.

15. Institutional review board (IRB) approvals or equivalent for research with human subjects

Question: Does the paper describe potential risks incurred by study participants, whether such risks were disclosed to the subjects, and whether Institutional Review Board (IRB) approvals (or an equivalent approval/review based on the requirements of your country or institution) were obtained?

Answer: [N/A]

Justification: The paper does not involve human-subject research, crowdsourcing, collection of personal data, or interaction with study participants. Therefore, IRB or equivalent approval is not applicable.

16. Declaration of LLM usage

Question: Does the paper describe the usage of LLMs if it is an important, original, or non-standard component of the core methods in this research? Note that if the LLM is used only for writing, editing, or formatting purposes and does *not* impact the core methodology, scientific rigor, or originality of the research, declaration is not required.

Answer: [N/A]

Justification: LLMs are not used as a component of MaSC, the experiments, or the metric computation. GPT-4V and GPT-4o appear only as comparator baselines, not as part of MaSC itself. Any use of LLMs during the project was limited to writing assistance and code-implementation help (analogous to standard developer tooling) and did not affect the formulation of the metric, the experimental design, the interpretation of results, or the originality of the research.